

This discussion paper is/has been under review for the journal Atmospheric Measurement Techniques (AMT). Please refer to the corresponding final paper in AMT if available.

Rainfall measurement from opportunistic use of earth-space link in Ku Band

L. Barthès and C. Mallet

Université de Versailles Saint-Quentin, LATMOS-IPSL, UMR8190, CNRS-INSU,
Laboratoire Atmosphères Milieux, Observations Spatiales, Quartier des Garennes,
11 Boulevard d'Alembert, 78280 Guyancourt, France

Received: 28 November 2012 – Accepted: 12 December 2012 – Published: 26 February 2013

Correspondence to: L. Barthès (laurent.barthes@latmos.ipsl.fr)

Published by Copernicus Publications on behalf of the European Geosciences Union.

Rainfall measurement from opportunistic use of earth-space link

L. Barthès and C. Mallet

Title Page

Abstract

Introduction

Conclusions

References

Tables

Figures



Back

Close

Full Screen / Esc

Printer-friendly Version

Interactive Discussion

Abstract

The present study deals with the development of a low cost microwave device devoted to measure average rain rate observed along earth – satellite links. The principle is to use rain atmospheric attenuation along Earth – space links in Ku-band to deduce the path averaged rain rate. These links are characterized by a path length of a few km through the troposphere. Ground based power measurements are carried out by receiving TV channels from different geostationary satellites in Ku-band.

The major difficulty in this study is to retrieve rain characteristics among many fluctuations of the received signal which are due to atmospheric scintillations, changes in the composition of the atmosphere (water vapour concentration, cloud water content) or satellite features (variation of the emitted power, satellite motions). In order to perform a feasibility study of such a device, a measurement campaign has been performed for five months near Paris. This paper proposes an algorithm based on an artificial neural network to identify drought and rainy periods and to suppress the variability of the received signal due to no-rain effects. Taking into account the height of the rain layer, rain attenuation is then inverted to obtain path averaged rain rate. Obtained rainfall rates are compared with co-located rain gauges and radar measurements on the whole experiment period, then the most significant rainy events are analyzed.

1 Introduction

Accurate measurements at medium scale rain intensity and precise localization of precipitation are an important task for the study of the water cycle, and it is also a major element of the physics of climate. Moreover, issues concerning the variability of precipitation in time and space are not only scientific. Knowledge of rainfall variability in the short term (extreme events), and long term (management of water resources), may also help to reduce the human and material damage caused by these phenomena.

Rainfall measurement from opportunistic use of earth-space link

L. Barthès and C. Mallet

Title Page

Abstract

Introduction

Conclusions

References

Tables

Figures

⏪

⏩

◀

▶

Back

Close

Full Screen / Esc

Printer-friendly Version

Interactive Discussion



Rainfall measurement from opportunistic use of earth-space link

L. Barthès and C. Mallet

Title Page

Abstract

Introduction

Conclusions

References

Tables

Figures

⏪

⏩

◀

▶

Back

Close

Full Screen / Esc

Printer-friendly Version

Interactive Discussion

significantly to absorption in the microwave spectrum. In the case of a satellite slant path, gaseous absorption can be considered to be homogeneous over the horizontal range of a link and variations in gas-induced attenuation are mainly due to variations in water vapor quantity. Gaseous attenuation can not exceed 0.3 dB at frequencies near 10 GHz and elevation angle of 30° (ITU P.676-9, 2012).

The interaction of electromagnetic wave with tropospheric water particles may involve both absorption and scattering depending their size relatively to the wavelength. Attenuation per unit of volume depends on the density, shape, size distribution, and dielectric properties of the particles contained in the volume. Concerning clouds liquid water, scattering is negligible and the Rayleigh approximation can thus be considered for frequencies up to about 50 GHz (Liebe et al., 1993), the resulting attenuation is proportional to the integrated liquid water content present along the link.. As cloud coverage exhibit important spatiotemporal variability, the corresponding liquid content varies substantially and cloud-induced attenuation can vary strongly but remains below 1 dB for frequencies and elevation angles considered in this study (ITU P840-5, 2012). Concerning ice particles, their absorption coefficient is much smaller than that of water and they do not play a significant role in Ku-band. Rain is the major contributor to attenuation in Ku-band, both absorption and scattering phenomena play an important role. The attenuation per unit of volume depends on extinction cross section of the water particles and their size distribution profile. This latter varies noticeably both in space and time involving a specific dynamic of rain-induced attenuation which is different from gases or cloud ones.

2.1 Rain – atmospheric attenuation relationship

Considering scattering effects, the rain specific attenuation $k_{f,p\theta}(t,l)$ [dB km⁻¹] is related to rain microphysics properties for a given frequency f , polarization p ($p = H, p = V$ or $p = C$ for horizontal, vertical or circular polarization respectively) and an elevation angle θ by the following relation:

Rainfall measurement from opportunistic use of earth-space link

L. Barthès and C. Mallet

Title Page

Abstract

Introduction

Conclusions

References

Tables

Figures

⏪

⏩

◀

▶

Back

Close

Full Screen / Esc

Printer-friendly Version

Interactive Discussion

$$k_{f\rho\theta}(t, l) = 4343 \int_{D_{\min}}^{D_{\max}} N(D, t, l) \sigma_{f\rho\theta}(D) dD$$

Where $N(D, t, l)$ [m^{-4}] is the rain drop size distribution (DSD), i.e. the number of drops per cubic meter per unit increment of diameter D , present in the atmosphere at location l and at time t , $\sigma_{f\rho\theta}(D)$ [m^2] is the extinction cross-section for a raindrop of diameter D [m].

The rain attenuation $A_{f\rho\theta}^{\text{Rain}}(t)$ [dB] is thus obtained by integrating the specific attenuation along the slant path of length L :

$$A_{f\rho\theta}^{\text{Rain}}(t) = \int_0^L k_{f\rho\theta}(t, l) dl$$

The extinction cross section $\sigma_{f\rho\theta}(D)$ of raindrops depends on the used frequency, the refractive index n of the water, the size and the shape of the raindrops, the polarization and the incidence angle of the electromagnetic wave. In this study, we consider that $\sigma_{f\rho\theta}(D)$ is independent of location l even if during the drop fall, the temperature and/or pressure variations can lead to a slight variation of the refractive n . We assume in this study, that the induced variations of $\sigma_{f\rho\theta}(D)$ are negligible (Atlas, 1977). Under these conditions, profile of rain along the slant path of length L can be considered as a single layer of rain with an equivalent drop size distribution $N_e(D, t)$ [m^{-4}], defined by:

$$N_e(D, t) = \frac{1}{L} \int_0^L N(D, t, l) dl$$

We can express the equivalent specific attenuation $k_{f\rho\theta}(t)$:

$$k_{f\rho\theta}(t) = 4343 \times \int_{D_{\min}}^{D_{\max}} N_e(D, t) \sigma_{f\rho\theta}(D) dD \quad (1)$$

Simply related to rain attenuation as follow:

$$A_{f\rho\theta}^{\text{Rain}}(t) = k_{f\rho\theta}(t) \times L \quad (2)$$

5 In practice, the DSD is generally unknown but, considering a gamma drop size distribution the following k - R empirical power law relation between the specific attenuation and rain rate is used instead:

$$k_{f\rho\theta}(t) = a_{f\rho\theta} \times R^{b_{f\rho\theta}}(t) \quad (3)$$

10 This expression is shown to be an approximation, except in the low frequency and optical limits (Olsen, 1978). In the field of microwave $a_{f\rho\theta}$ and $b_{f\rho\theta}$ depend on frequency and to a lesser extent to the drop size distribution, elevation angle and polarisation.

2.2 Accuracy of the k - R power law relationship

As we have seen above, k - R relation depends on the equivalent DSD features that are to say, drops concentration and shape. These features depend both to atmospheric conditions (convective or stratiform rain for example) and their variability along the radio link L (i.e. the considered spatial scale).

15 We first consider a homogeneous layer with different concentrations and shapes. As pointed out by Jameson (1991) the dependency to the shape for a homogeneous rain layer is related to the frequency. For frequencies close to 25 GHz, the authors show the dependency is weak while larger dispersion appears for lower frequencies especially for $f < 9$ GHz. In our case the use of 12 GHz links will be expected to be more or

Rainfall measurement from opportunistic use of earth-space link

L. Barthès and C. Mallet

Title Page

Abstract

Introduction

Conclusions

References

Tables

Figures

⏪

⏩

◀

▶

Back

Close

Full Screen / Esc

Printer-friendly Version

Interactive Discussion



Rainfall measurement from opportunistic use of earth-space link

L. Barthès and C. Mallet

Title Page

Abstract

Introduction

Conclusions

References

Tables

Figures



Back

Close

Full Screen / Esc

Printer-friendly Version

Interactive Discussion



less sensitive to rain microphysics. To assess its impact, 1-min drops size distributions have been computed from rain drops data set collected by a disdrometer (Delahaye et al., 2006) over a period of 24 months between July 2008 and July 2001. By using an approach similar to Leijnse et al. (2010), for each DSD the corresponding rain rate values R and specific attenuation values k_{fp} (Eq. 1) were calculated for a frequency of 12 GHz using Mie theory (considering drops shape as spherical). The temperature is taken equal to 10° C and as rain drops are considered as spherical, obtained specific attenuations are not polarized dependants. Figure 1 shows the obtained scatter plot, the solid line shows the obtained fitted power law and the dashed curve allows comparison with the power law model given by the standard International Telecommunication Union recommendation (ITU-R P.618-9). We can see that the two curves are very similar and are difficult to distinguish from each other. As it can be seen on the figure discrepancy due to microphysics can cause an error of more or less $\pm 7 \text{ mm h}^{-1}$ for rain rates greater than 10 mm h^{-1} . More precisely, rain rate standard deviation varies from 0.2 to 6 mm h^{-1} for rain rate ranging from 1 to 100 mm h^{-1} leading respectively to relative standard deviations (RSD) between 20 % to 6 %. This result confirm that the use of a 12 GHz frequency is not optimal for the restitution of low rain rate and thus the proposed device should rather be used for applications for which stronger rain events are relevant (flash flood forecast for example). Table 1 column 2 shows the obtained coefficients by performing the linear regressions on $\log(k) - \log(R)$. These coefficients are very similar to those given by ITU model (Table 1 column 7, 8 and 9).

Concerning the variability of the DSD along the radio link, the k – R relations are expected to be sensitive to aggregation over domains of different volumes. Numerous study, that concern radar measurements, have been devoted to the Z – R power laws relationships between the reflectivity Z and the rain rate R . Morin et al. (2003) have shown empirically the existence of a scale dependency of Z – R law parameters based on the study of collocated radar and rain gauge data aggregated at different spatial scales. These authors found a quick increase of parameter a with scale as well as a moderate decrease of the parameter b . Recently Verrier et al. (2012, 2013) quantified

the impact of scaling properties of rainfall on $Z-R$ relations using multifractal theory. These authors found that if multifractality behaviour simultaneously holds for R and Z , the $Z-R$ relationships are characterized by:

$$\begin{cases} b = \text{constant} \\ a \propto K_R^{(b)} \end{cases} \quad (4)$$

5 where $K_R(q)$ defines the “moment scaling function” that entirely characterizes the statistics of the rain field. Usually, $K_R(q)$ is determined by the knowledge of a reduced set of “universal” parameters (Schertzer and Lovejoy, 1987). The coefficient a should therefore be power-law of scale, with scaling exponent that can be demonstrated (from multifractal theory) to be positive when $b > 1$ and negative when $b < 1$. So as to quantify the impact of scaling properties of rainfall on $k-R$ relations the study performed by Verrier et al. (2012, 2013) relatively to the $Z-R$ relationships is applied to the $k-R$ relationships. With a hypothesis of “frozen” atmosphere it can be considered that increasing integration time is equivalent to consider larger spatial scales and thus to obtained $k-R$ relations at different spatial scales. The rain drops dataset previously presented was used again to compute DSD with integration times varying between 1 and 60 min and the corresponding $k-R$ relations were computed. Note that the rain rate series have been previously demonstrated to follow multifractal statistics at mesoscale and submesoscale in a detailed study (Verrier et al., 2011). In Table 1, the stability of the obtained coefficients associated with the high values of the determination coefficients ($R^2 \geq 0.972$) shows that the $k-R$ relation is quite insensitive to integration time and thus to spatial scale (for the considered frequency). The robustness of the $k-R$ relationship is due to the fact that exponent b is close to 1 (1.17) leading to a less critical to scale dependency of $k-R$ relationships parameters than for the $Z-R$ relationships for which b is close to 1.6. More precisely, in our case $K_R(1.17)$ is equal to 0.03 while $K_R(1.6)$ is equal to 0.12 for reflectivity radar. When considering for example integration times of 1 and 10 min, these values lead to a ratio of the prefactor a for $k-R$ and $Z-R$ relationships respectively equal to 1.07 and 1.31. The latter value show that spatial

Rainfall measurement from opportunistic use of earth-space link

L. Barthès and C. Mallet

Title Page

Abstract

Introduction

Conclusions

References

Tables

Figures



Back

Close

Full Screen / Esc

Printer-friendly Version

Interactive Discussion



Rainfall measurement from opportunistic use of earth-space link

L. Barthès and C. Mallet

Title Page

Abstract

Introduction

Conclusions

References

Tables

Figures

◀

▶

◀

▶

Back

Close

Full Screen / Esc

Printer-friendly Version

Interactive Discussion

scale variability can conduct in the case of radar to an important error in some meteorological situations. Concerning the coefficient b , Table 1 shows it is almost constant (relative error $< 3.5\%$) as predict by the theory. The stability of the $k-R$ relation deduce from scale properties is relatively well confirmed by empirical values given in Table 1 from 1 to about 30 min which correspond to spatial scales between few hundred meters to few km in accordance with the path length L . The $k-R$ estimated parameters are very close to those of the ITU (Recommendation ITU-R P.618-9), for this reason they will be used in the following of the study. Figure 2 shows error statistics between specific attenuations computed from Eq. (1) and those obtained with Eq. (3) and ITU coefficients. A five minutes integration time is selected in order to represent a spatial scale in accordance with Earth – satellite length path L . Obtained bias is comprised between 1 and -6 mm h^{-1} with an absolute relative error less than 10%.

3 Experimental setup

The experimental system was set up at the LATMOS (Laboratoire Atmosphères, Milieux, Observations Spatiales) in Guyancourt, near Paris, during the summer and autumn 2010. Signals from four geostationary satellites (NSS7, AB1, Thor 5/6, Hotbird 6/8/9) have been received in horizontal polarization, with a multifocus dish antenna of 90 cm diameter. The elevations of link path are closed to 30° . For each satellites two 30 MHz width Ku-band channels were received and downconverted by four low-noise block converter (LNBC) to L-band signals. A RF Switch allows selecting sequentially one of the L-band signals before to feed a field analyser. The latter has an accuracy of 0.1 dB and operates in spectrum mode with a 4 MHz bandwidth centered sequentially on the selected channels. The measured level is obtained by averaging five consecutive measurements, then the averaged value is saved by a micro calculator which is used as a data logger. The acquisition sequence records sequentially each of the 8 channels with a sampling period of 2 s per channel leading to a total period of 16 s (4 satellites \times 2 channels \times 2 s). Figure 3 shows the experimental set up. The frequencies

of each link are given in Table 2. Note that influence of wet antenna (Leijnse et al., 2008) is not taken into account here, we simply applied a special spray on the LNBS to help removing the droplets. Moreover in the case of Earth-space microwave links only the ground antenna can be wetted.

Independent co-located rain observations are also considered to evaluate the performances of the proposed Ku device: near-by C-band weather radar rain-rate maps provided by Météo France located at Trappes and two rain gauges located at Trappes and Toussus le Noble. The distances between the LATMOS and these places are respectively 2.9 and 3.7 km. Figure 4 shows the different locations and the directions of the four earth-satellites links (blue lines). The dataset is summarized below:

- 8 time series of received signal $P_{\text{REC}}^{\text{ch}}$ with ch equal 1 to 8 (4 satellites and 2 channels for each satellite) with a 10 s sampling resolution obtained by applying a re-sampling algorithm to the original times series.
- 2 hourly accumulated rainfall time series $R^{\text{RG1}}(t)$ and $R^{\text{RG2}}(t)$ obtained with the two rain gauges.
- 20 000 radar rain rate maps $R^{\text{rad}}(t)$ with a spatial resolution of $1 \times 1 \text{ km}^2$ and temporal resolution of 5 min. The relation employed to convert radar reflectivity factors to rain rate is the one used operationally by Météo-France (Tabary, 2007). The period considered covers most of the rainfall events from 23 July to 15 December 2010.

In this first feasibility study, each of the 8 available channels is used independently. Channel 1 is used for the development of algorithms (see Sect. 4), thus seven different values of rain rate are then estimated from other channels. As results obtained with each of the seven remaining channels are quite similar, only those obtained with channel 7 are presented in Sect. 5.

Since microwave links provide path integrated measurements, the corresponding radar path averaged rain rates are calculated from rain maps by averaging the radar

Rainfall measurement from opportunistic use of earth-space link

L. Barthès and C. Mallet

Title Page

Abstract

Introduction

Conclusions

References

Tables

Figures

⏪

⏩

◀

▶

Back

Close

Full Screen / Esc

Printer-friendly Version

Interactive Discussion



pixels $R_i^{\text{rad}}(t)$ crossed by the link beam weighted by the corresponding length of the link L_i in the pixel.

For each of the 8 received channels ch and each available radar maps $R^{\text{rad}}(t)$ the radar average rain rate along the earth-satellite path corresponding to channel ch is

5 thus given by : $\bar{R}_{ch}^{\text{rad}}(t) = \frac{\sum_{i \in I} L_i R_i^{\text{rad}}(t)}{\sum_{i \in I} L_i}$ where $R_i^{\text{rad}}(t)$ is the i th pixel ($i \in [1, 262\ 144]$) of the

map, I is the subset of pixels that intersects the path of the satellite corresponding to channel ch , and L_i is the length of the link inside the pixel i .

Finally, 4 times series $\bar{R}_{ch}^{\text{rad}}(t)$ were obtained with a 5 min temporal resolution representing path averaged rain rates on each earth-satellite links according to radar measurements.

10 Concerning rain gauges we simply averaged the two time series $R^{\text{RG1}}(t)$ and $R^{\text{RG2}}(t)$ to obtain $\bar{R}^{\text{RG}}(t)$. Figure 5 shows the time series $P_{\text{REC}}^{\text{ch1}}(t)$, $\bar{R}_{ch1}^{\text{rad}}(t)$, $\bar{R}_{\text{RG}}(t)$ for a 10 days period.

15 Rainy periods are clearly characterized by a local decrease of the received signal, they thus appear as negative pulses. At the same time, precipitations are also visible on the radar and rain gauges time series. It is also important to note the significant daily variation of the signal (~ 1 dB) due to satellite motion and antenna aperture as well as a negative trend due to a decrease of temperature and/or water vapour content. For all these reasons, it is very difficult to estimate directly a reference level and thus
20 to deduce the rain attenuation. As explained in the next section, the estimation of the reference level requires first to detect the drought periods from rainy periods taking into account the variability of the signal.

Rainfall measurement from opportunistic use of earth-space link

L. Barthès and C. Mallet

Title Page

Abstract

Introduction

Conclusions

References

Tables

Figures



Back

Close

Full Screen / Esc

Printer-friendly Version

Interactive Discussion

4 Retrieval method

4.1 Reference level

The level of the received signal (P_{REC}) results from the combination of instrumental and geometric characteristics such as power of the transmitter (P_{E}) on-board the satellite, transmitter and receiver antennas gain G_{E} , G_{R} , free space attenuation A_{F} and tropospheric attenuation (A^{Trop}).

$$P_{\text{REC}}(t) = P_{\text{E}}(t) + G_{\text{E}}(t) + G_{\text{R}}(t) - A_{\text{F}}(t) - A^{\text{Trop}}(t)(\text{dB}) \quad (5)$$

In practice, P_{E} and G_{E} are almost always constants while G_{R} and A_{F} vary slowly over time due to satellite motion. Tropospheric attenuation A^{Trop} is critically dependent upon satellite elevation and frequency band. In Ku-band as has been stated previously, rain is the dominant contributor to attenuation (A^{Rain}) even if oxygen (A^{Oxygen}), liquid water in clouds (A^{Cloud}), and water vapor (A^{Vapor}) and scintillation (A_{S}) are also present:

$$A^{\text{Trop}}(t) = A^{\text{S}}(t) + A^{\text{Oxygen}}(t) + A^{\text{Cloud}}(t) + A^{\text{Vapor}}(t) + A^{\text{Rain}}(t)(\text{dB})$$

In order to estimate rain attenuation (A^{Rain}), Eq. (5) is expressed as follows:

$$P_{\text{REC}}(t) = P_{\text{REF}}(t) - A^{\text{Rain}}(t)(\text{dB}) \quad (6)$$

where $P_{\text{REF}}(t)$, called reference level or baseline, is equal to:

$$P_{\text{REF}}(t) = P_{\text{E}} + G_{\text{E}} + G_{\text{R}} - A_{\text{F}} - A^{\text{S}}(t) - A^{\text{Oxygen}}(t) - A^{\text{Cloud}}(t) - A^{\text{Vapor}}(t)(\text{dB})$$

In no-rainy situations, we have:

$$P_{\text{REC}}(t) = P_{\text{REF}}(t)(\text{dB})$$

The reference level is directly observed during non-rainy situations, it is therefore necessary to estimate it during rain events from reference level obtained during dry periods. It is thus essential to dispose of an algorithm allowing differentiating the drought

Rainfall measurement from opportunistic use of earth-space link

L. Barthès and C. Mallet

Title Page

Abstract

Introduction

Conclusions

References

Tables

Figures

⏪

⏩

◀

▶

Back

Close

Full Screen / Esc

Printer-friendly Version

Interactive Discussion



and rainy periods. After the reference level is known, Eqs. (2), (3) and (6) allow estimating the corresponding rain rate $\bar{R}_{ch}^{KU}(t)$.

4.2 The rain – no rain detection algorithm

Each of the atmospheric processes involved has its own dynamics and contributes differently to the wave attenuation. Because of the high heterogeneity of the rain, the latter causes temporal fluctuations faster than gases or clouds of the received signal. To separate drought from rainy periods a similar approach to those used by Kaufmann and Rieckermann (2011) and Schleiss and Berne (2010) was used. Different characteristics (trends, standard deviation, kurtosis, skewness) of the observed Ku-band signal received on channel 1 have been computed using different window size from 100 s to one hour. Radar data

have been used to determine the corresponding state of the atmosphere (rainy or dry). The statistical distributions of these characteristics for rainy and dry periods have been compared to test their ability to discriminate between the two states. If it is centered on the time t to which the rainfall rate is estimated, the window width W should not be chosen too large since it determines the time delay necessary to obtain the estimate. As our goal is to develop, as far as possible, a sensor that allows near real time observation we chose the time windows as small as possible but still guaranteeing good discrimination.

Two characteristics have thus been selected (see Eq. 7): the standard deviation over a time window equal to 30 mn and the local trend over a time window equal to 4 mn.

$$\left\{ \begin{array}{l} \text{std}(P_{\text{REC}}(n)) = \left[\frac{1}{2W+1} \sum_{i=-L}^L (P_{\text{REC}}(n+i) - \bar{P}_{\text{REC}}(n))^2 \right]^{\frac{1}{2}} \quad \text{with } \bar{P}_{\text{REC}}(n) = \frac{1}{2W+1} \sum_{i=-L}^L P_{\text{REC}}(n+i) \quad \text{and } W=100 \\ \text{Trd}(P_{\text{REC}}(n)) = \frac{1}{W} \sum_{i=-L}^L a_i P_{\text{REC}}(n+i) \quad \text{with } a = (-1, -1, \dots, -1, 0, 1, \dots, 1) \quad \text{and } W=10 \end{array} \right. \quad (7)$$

Our aim was to obtain a pattern classifier that provides a rule for assigning each sample $P_{\text{REC}}(n)$ to one of the two classes (rainy or dry). Because the optimal boundary

Rainfall measurement from opportunistic use of earth-space link

L. Barthès and C. Mallet

Title Page

Abstract

Introduction

Conclusions

References

Tables

Figures

⏪

⏩

◀

▶

Back

Close

Full Screen / Esc

Printer-friendly Version

Interactive Discussion



Rainfall measurement from opportunistic use of earth-space link

L. Barthès and C. Mallet

Title Page

Abstract

Introduction

Conclusions

References

Tables

Figures

⏪

⏩

◀

▶

Back

Close

Full Screen / Esc

Printer-friendly Version

Interactive Discussion

where h_R is the rain height given by ITU-R P 530-9 recommendation. The parameter h_S is the altitude of the ground station and θ the elevation angle. Finally, Eq. (3) gives the corresponding rain rate $\overline{R}_{ch1}^{KU}(t)$. The probability threshold P_o (found to be equal to 0.55) is chosen so that the obtained CDF of 1-h accumulated $\overline{R}_{ch1}^{KU}(t)$ is as close as possible to that of $\overline{R}_{ch1}^{rad}(t)$ (see Fig. 8). One can note that this threshold gives a percentage of rain similar to that obtained with a disdrometer during the same period located at 10 km of the receiver when a threshold of 0.1 mm h^{-1} is applied.

5 Validation and results

The method previously described is used to estimate \overline{R}_{ch7}^{KU} . Characteristics vector \mathbf{X} , corresponding to channel 7, has been computed from the time series P_{REC}^{ch7} and is applied to the MLP. The threshold P_o allows identifying rainy and dry periods. In order to quantify the performance of the device and associated algorithm, comparison with $\overline{R}_{ch7}^{rad}(t)$ and $\overline{R}^{RG}(t)$ are then performed using different criteria. First, a visual comparison of the obtained times series of rainfall intensities measured by the radar and the Ku device is performed, the order of magnitude and the dynamics of the two measurements are similar (Fig. 9) even if these two quantities cannot be rigorously equal because of the different sampling volumes, altitudes and time resolutions. Figure 10 shows the comparison of accumulated rainfall measured by the gauges, the radar and those estimated from the received signal for the 4 months period. The radar and the Ku device obtained the same quantity with a total accumulated height of 220 mm while rain gauges measured a slightly higher value.

Figure 11 shows the comparison of hourly-accumulated rainfall measured by Radar and Ku device (top) and by rain gauge and Ku device (bottom). The quantile – quantile plots (left side) are relatively close to the diagonal indicating that the distributions of 1-h accumulated rainfall are quite similar. Right plots show error box plot. The medians are

close to zero especially between Ku device and radar except for intermediate cumulated rainfall (-1.3 mm). For both box plots, the width of the boxes defined as the width between the 25th and 75th percentiles increases as the cumulated rainfall increases, some explanations are proposed in the next paragraph.

5 Rain events case studies

Eight rain events of various intensities and durations have been selected. Although we cannot consider they are representative of the local rainfall climatology, they nonetheless allow to highlight a few points. The dates, durations, maximum rain rates and rain amounts estimated by the radar, the pluviometers and Ku device are given in Table 3.

10 Events are sorted by increasing duration. Note that the maximum rain rates R_{\max} are obtained with different integration time depending the device (Rain gauges: 1 h, Radar: 5 mn, Ku device 1 s). It can be seen that rain amount estimated by the radar and the sensor are relatively close to each other (deviation $< 15\%$) for events whose duration are between 1 and 3 h (Events #3, 4, 5, 6). This is not the case for short (< 1 h) nor for
15 long duration events (> 6 h). For events of short duration (Events #1, 2) the maximum values R_{\max} between radar and Ku device are relatively close to each other, but it is difficult to compare the rain amount because of the small size of the rain-cells. Indeed, for small rain-cells crossed more or less perpendicularly by the microwave link, the cell is seen only during a few seconds or minutes while the cell is seen longer in the corresponding pixel radar because its size is much more larger (1 km) than the microwave link (few meters). Thus the two instruments have not necessarily seen the same thing. For long duration rain events (Events #7, 8), the reason is completely different, it appears that the basic interpolation method used for the calculation of the reference level is not suitable and a more sophisticated method should be used. It should be noted that
20 in all cases, the comparison between the devices remains difficult for several reasons: (i) it is well known that radar $Z-R$ equation sometimes overestimates or underestimates the rain rate, (ii) path length L can be under or overestimated if isotherm zero

Rainfall measurement from opportunistic use of earth-space link

L. Barthès and C. Mallet

Title Page

Abstract

Introduction

Conclusions

References

Tables

Figures



Back

Close

Full Screen / Esc

Printer-friendly Version

Interactive Discussion



is not sufficiently well known, (iii) in presence of high rainfall rates which correspond to very strong spatial heterogeneities they can lead to significant differences because the instruments do not see the same volume.

6 Conclusions

Ku-band microwave sources on board of satellites such as those employed in telecommunication or broadcasting can potentially be used for the estimation of rainfall. A ground low cost microwave system able to estimate atmospheric attenuation along earth to satellite links has been developed to investigate an opportunistic use of these microwave sources in the band 10.7–12.7 GHz. Although this band is not optimal for estimating weak rainfall rates due to its lack of sensitivity, it seems to be a good choice when the rainfall rate increases because the attenuation rarely exceeds 12 dB even in presence of very heavy rains, and it remains easily measurable even with a parabola of standard size (90 cm).

A 4 months measurement campaign was performed. A Multi-Layer Neural Network was proposed to identify dry and rainy periods from the received signal and thus to estimate the attenuation due to rain on the path link. ITU models were then used to convert rain attenuation into rainfall rate. Good agreement between the Ku device, weather radar and rain gauge in term of total accumulated rainfall but also in term of hourly rainfall distribution is obtained. Concerning 1-h cumulated rainfall, discrepancies up to 30 % can occur between radar and Ku device. This can be explained by the large difference in sample volume and time integration of the two devices which do not “see” the same thing during heavy rainfall events which are generally associated to very strong spatial heterogeneities. Although the presented results constitute only a partial validation and despite the simplicity of some models and the use of empirical formulas, these first results are promising. It is difficult to compare our results with those obtained by Maitra et al. (2007) who compared rain attenuations with a co-localized disdrometer and a Simple Attenuation Model (SAM) (Stutzman and Yon, 1986). They conclude that

Rainfall measurement from opportunistic use of earth-space link

L. Barthès and C. Mallet

Title Page

Abstract

Introduction

Conclusions

References

Tables

Figures



Back

Close

Full Screen / Esc

Printer-friendly Version

Interactive Discussion



“the discrepancy becomes significant when the rain rates are large (above 30 mm h^{-1}) and the corresponding rain cell size is small”. The authors explain that for large rain rates, the rain rate decay parameter used in the SAM is not still valid and consequently nothing can be concluded.

Several possibilities could be investigated to improve the performances. In this first feasibility study, each of the available channel (i.e. one frequency and one polarization), is used independently to estimate different values of rain rate. In the future, the combined use of several channels corresponding to different frequencies or polarizations should improve the performances. For long duration rain events ($> 3 \text{ h}$) improvements are still needed, especially in the evaluation of the reference level. Indeed, in this study a simple linear interpolation from dry periods was used. This is only sufficient for short periods in which reference level has little variations. A more sophisticated estimation of the reference level has to be performed for example by representing the reference level with a state-space model associated with a Kalman filter. ITU models were used for the $k-R$ relation and for the estimation of the path length. According to our study the ITU $k-R$ relation perfectly suit to our problem, but we do not knowing about the path length. Other models exist like the one proposed by Adhikari et al. (2011) and should be tested.

The present study deals with the estimation of rainfall rate from a single path link. In the future, the use of several simultaneous links associated with tomography or assimilation methods by using approach similar to Zinevich et al. (2008, 2009) or Giulli et al. (1997, 1999) could be used to estimate rainfall fields at small-scale and could be helpful in hydrology, flash flood forecasting or for weather radar calibration.

Acknowledgements. The authors would like to thank M. Parent du Chatelet from Météo France for the various conversations we had on radar data processing.

Rainfall measurement from opportunistic use of earth-space link

L. Barthès and C. Mallet

Title Page

Abstract

Introduction

Conclusions

References

Tables

Figures



Back

Close

Full Screen / Esc

Printer-friendly Version

Interactive Discussion



Rainfall measurement from opportunistic use of earth-space link

L. Barthès and C. Mallet

Title Page

Abstract

Introduction

Conclusions

References

Tables

Figures

◀

▶

◀

▶

Back

Close

Full Screen / Esc

Printer-friendly Version

Interactive Discussion

- Messer, H., Zinevich, A., and Alpert, P.: Environmental monitoring by wireless communication networks, *Science*, 312, 713–716, 2006.
- Morin, E., Krajewski, W. F., Goodrich, D., Xiaogang, G., and Sorooshian S.: Estimating rainfall intensities from weather radar data: the scale-dependency problem, *J. Hydrometeorol.*, 4, 782–797, 2003.
- Olsen, R. L., Rogers, D. V., and Hodge, D. B.: The aRb relation in the calculation of the rain attenuation, *IEEE Conf. Publ.*, 26, 318–329, 1978.
- Ramachandran, V. and Kumar, V.: Rain Attenuation Measurement on Ku-band Satellite TV Downlink in Small Island, *Electron. Lett.*, 40, 49–50, 2004.
- Schertzer, D. and Lovejoy, S.: Physically based rain and cloud modeling by anisotropic, multiplicative turbulent cascades, *J. Geophys. Res.*, 92, 9692–9714, 1987.
- Schleiss, M. and Berne, A.: Identification of dry and rainy periods using telecommunication microwave links, *IEEE Geosci. Remote Sens. Lett.*, 7, 611–615, doi:10.1109/LGRS.2010.2043052, 2010.
- Stutzman, W. L. and Yon, K. M.: A simple rain attenuation model for earth-space radio links operating at 10–35 GHz, *Radio Sci.*, 21, 65–72, doi:10.1029/RS021i001p00065, 1986.
- Tabary, P.: The new french operational radar rainfall product. Part I: methodology, *Weather Forecast.*, 22, 393–408, 2007.
- Ulaby, F. T., Moore, R. K., and Fung, A. K.: *Microwave Remote Sensing, Active and Passive, Vol. 1, Microwave Remote Sensing Fundamentals and Radiometry*, Artech house Inc., 1981.
- Upton, G. J. G, Holt, A. R., Cummings, R. J., Rahimi, A. R., and Goddard, J. W. F.: Microwave links: the future for urban rainfall measurement?, *Atmos. Res.*, 77, 300–312, 2005.
- Verrier, S., Mallet, C., and Barthès, L.: Multiscaling properties of rain in the time domain, taking into account rain support biases, *J. Geophys. Res.*, 116, D20119, doi:10.1029/2011JD015719, 2011.
- Verrier, S., Barthes, L., and Mallet, C.: Scaling properties of rainfall in space and time and their impact on rain rate estimation from weather radar 7th European Conference on Radar in Meteorology and Hydrology ERAD2012, Toulouse, France, 2012.
- Verrier, S., Barthes, L., and Mallet, C.: Theoretical and empirical scale-dependency of $Z-R$ relationships: evidence, impacts and correction, *J. Geophys. Res.*, submitted, 2013.
- Wang, Z., Schleiss, M., Jaffrain, J., Berne, A., and Rieckermann, J.: Using Markov switching models to infer dry and rainy periods from telecommunication microwave link signals, *Atmos. Meas. Tech.*, 5, 1847–1859, doi:10.5194/amt-5-1847-2012, 2012.

Zhang, G. P.: Neural Networks for Classification: A Survey, IEEE T. Syst. Man. C., 30, 451–462, 2000.

Zinevich, A., Alpert, P., and Messer, H.: Estimation of rainfall fields using commercial microwave communication networks of variable density, Adv. Water Res., 31, 1470–1480, 2008.

5 Zinevich, A., Messer, H., and Alpert, P.: Frontal Rainfall Observation by a Commercial Microwave Communication Network, J. Appl. Meteorol. Clim., 48, 1317–1334, 2009.

AMTD

6, 2113–2150, 2013

Rainfall measurement from opportunistic use of earth-space link

L. Barthès and C. Mallet

Title Page

Abstract

Introduction

Conclusions

References

Tables

Figures



Back

Close

Full Screen / Esc

Printer-friendly Version

Interactive Discussion



Rainfall measurement from opportunistic use of earth-space link

L. Barthès and C. Mallet

Table 1. Coefficients of linear regression and coefficients of determination obtained by performing the linear regressions on $-\log(k\theta) - \log(R)$ scatterplots for a frequency f equal to 12 GHz and integration times varying between 1 and 60 min. The three last columns indicate the ITU recommendation coefficients corresponding respectively to horizontal, circular and vertical polarizations at the same frequency.

	1 mn	5 mn	10 mn	30 mn	60 mn	ITU (H)	ITU (C)	ITU (V)
a	0.027	0.028	0.030	0.030	0.033	0.024	0.024	0.024
b	1.15	1.14	1.13	1.12	1.1	1.17	1.15	1.13
R^2	0.987	0.986	0.98	0.992	0.972	na	na	na

[Title Page](#)
[Abstract](#)
[Introduction](#)
[Conclusions](#)
[References](#)
[Tables](#)
[Figures](#)
[⏪](#)
[⏩](#)
[◀](#)
[▶](#)
[Back](#)
[Close](#)
[Full Screen / Esc](#)
[Printer-friendly Version](#)
[Interactive Discussion](#)


Rainfall measurement from opportunistic use of earth-space link

L. Barthès and C. Mallet

Table 2. Frequency [MHz] of the considered microwave links.

Channel	Satellite	Frequency	Channel	Satellite	Frequency
1	NSS7	12 604	5	Thor 5/6	12 563
2	NSS7	11 694	6	Thor 5/6	12 688
3	AB1	12 722	7	Hotbird 6/8/9	12 285
4	AB1	12 547	8	Hotbird 6/8/9	12 617

Title Page

Abstract

Introduction

Conclusions

References

Tables

Figures

◀

▶

◀

▶

Back

Close

Full Screen / Esc

Printer-friendly Version

Interactive Discussion



Rainfall measurement from opportunistic use of earth-space link

L. Barthès and C. Mallet

Table 3. Feature of the eight selected events.

Ev #	Date	Duration (h)	R_{\max} Rad (mm h ⁻¹)	R_{\max} Pluv (mm h ⁻¹)	R_{\max} Ku (mm h ⁻¹)	Amount Rad (mm)	Amount Pluv (mm)	Amount Ku (mm)
1	23 Jul	0.6	25.8	–	22.1	5.8	–	3
2	16 Oct	0.8	7.3	–	8.3	1.7	–	0.9
3	3 Oct	1.5	14.4	1.6	20.5	4.9	1.6	5.6
4	4 Aug	1.65	30.3	0.9	28.4	5.4	1	4.8
5	2 Aug	1.7	19.7	9.1	40	5.7	9.1	6.7
6	7 Sep	2.9	7.9	4.3	8.1	8.3	7	7.8
7	23 Aug	6.0	8.4	3.7	16.6	4.6	5.4	7.6
8	8 Nov	9.2	12.5	4	7.1	12.2	10.3	5.4

Title Page

Abstract

Introduction

Conclusions

References

Tables

Figures

⏪

⏩

◀

▶

Back

Close

Full Screen / Esc

Printer-friendly Version

Interactive Discussion

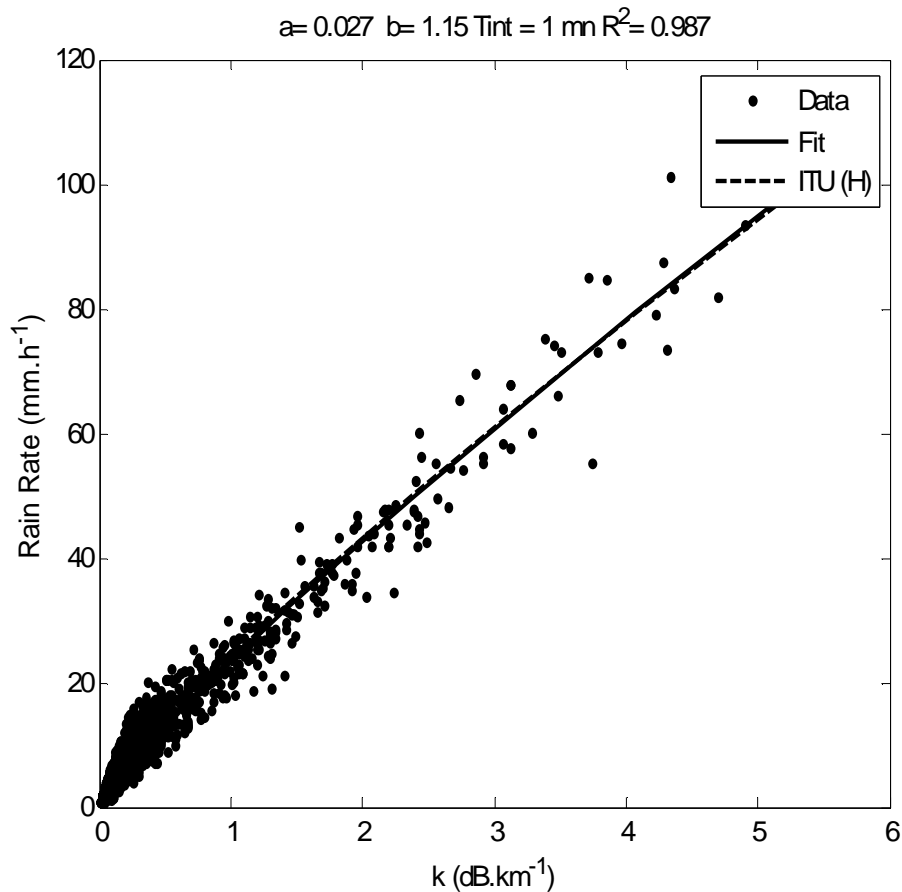


Fig. 1. Scatter plot of rain rate versus specific attenuation computed from drop size distribution and Mie theory for a frequency f equal to 12 GHz and a time resolution of 1 mm. The continuous line indicates the corresponding fitted k - R power law. The dotted line indicates the ITU power law for horizontal polarization.

Rainfall measurement from opportunistic use of earth-space link

L. Barthès and C. Mallet

Title Page

Abstract

Introduction

Conclusions

References

Tables

Figures

◀

▶

◀

▶

Back

Close

Full Screen / Esc

Printer-friendly Version

Interactive Discussion

Rainfall measurement from opportunistic use of earth-space link

L. Barthès and C. Mallet

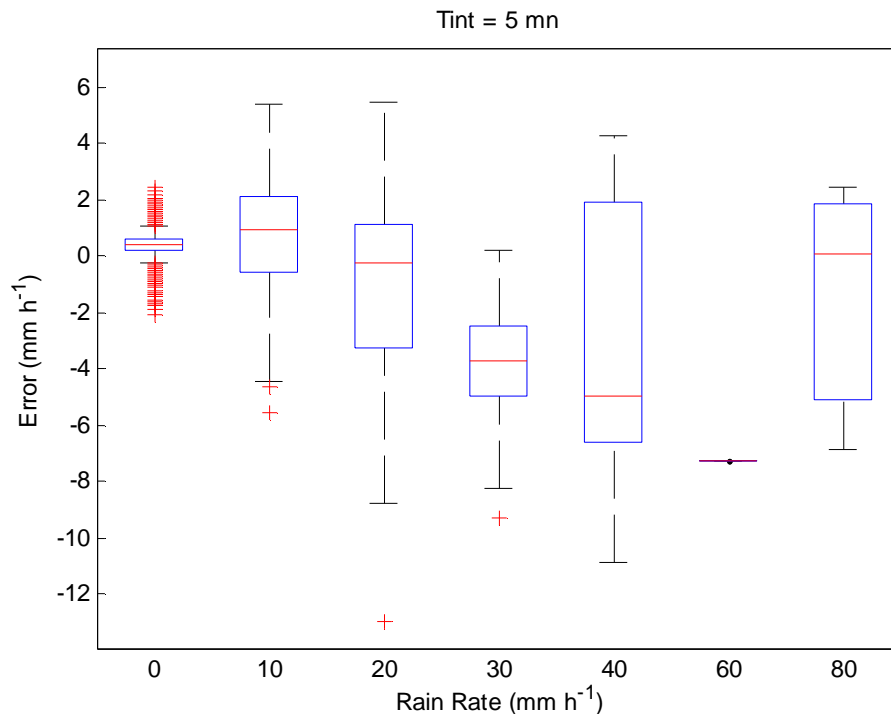


Fig. 2. Error induced on rain estimation when the ITU power law is used for an integration time equal to 5 mn. For each rain bin, the box-and-whiskers diagram indicates the median (the central vertical line), and the lower and upper quartiles (left and right edges of the box). The whiskers indicate the lower and upper limits of the distribution within 1.5 times the interquartile range from the lower and upper quartiles, respectively.

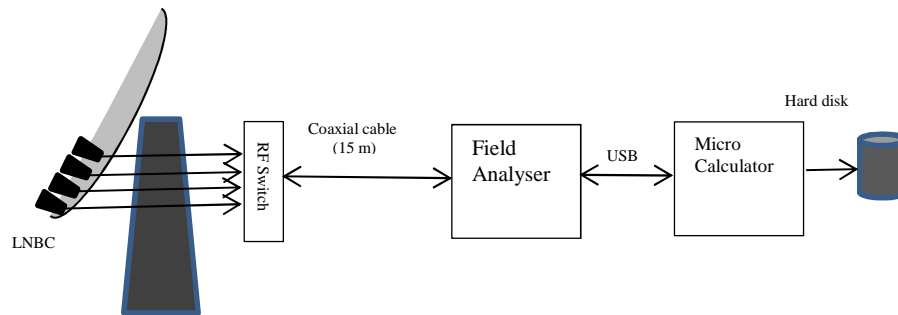


Fig. 3. Experimental setup.

Rainfall measurement from opportunistic use of earth-space link

L. Barthès and C. Mallet

Title Page	
Abstract	Introduction
Conclusions	References
Tables	Figures
⏪	⏩
◀	▶
Back	Close
Full Screen / Esc	
Printer-friendly Version	
Interactive Discussion	

AMTD

6, 2113–2150, 2013

Rainfall measurement from opportunistic use of earth-space link

L. Barthès and C. Mallet

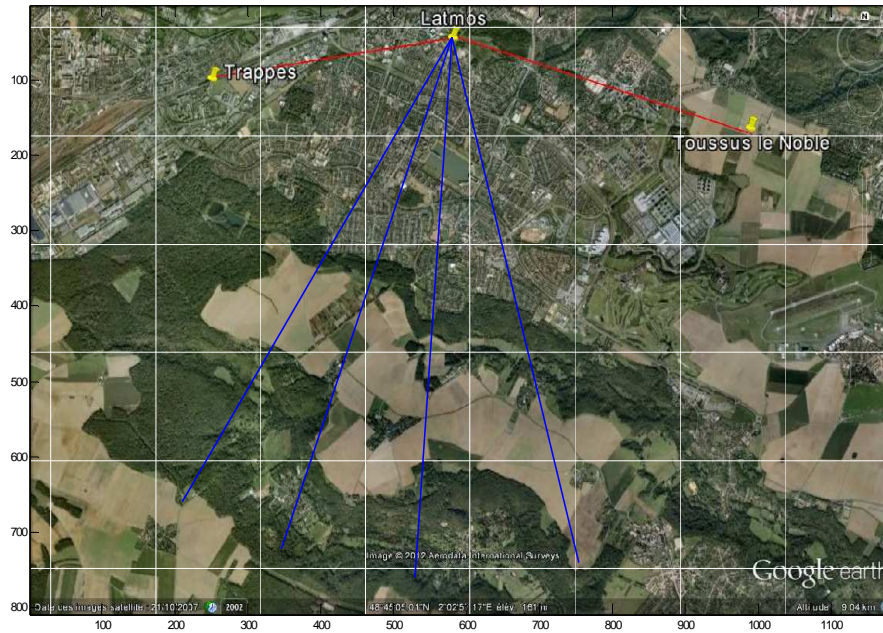


Fig. 4. Locations of the different sites and satellites path links.

[Title Page](#)
[Abstract](#)
[Introduction](#)
[Conclusions](#)
[References](#)
[Tables](#)
[Figures](#)
[⏪](#)
[⏩](#)
[⏴](#)
[⏵](#)
[Back](#)
[Close](#)
[Full Screen / Esc](#)
[Printer-friendly Version](#)
[Interactive Discussion](#)


Rainfall measurement from opportunistic use of earth-space link

L. Barthès and C. Mallet

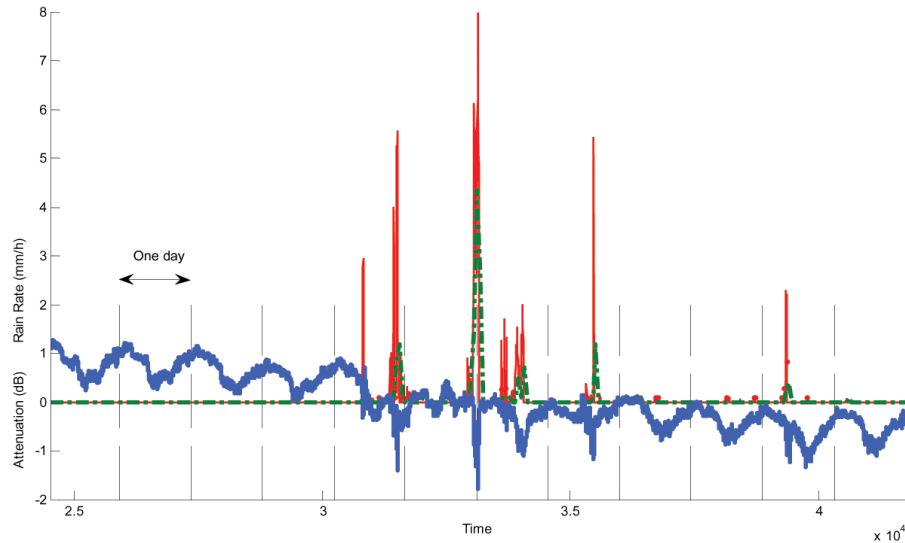
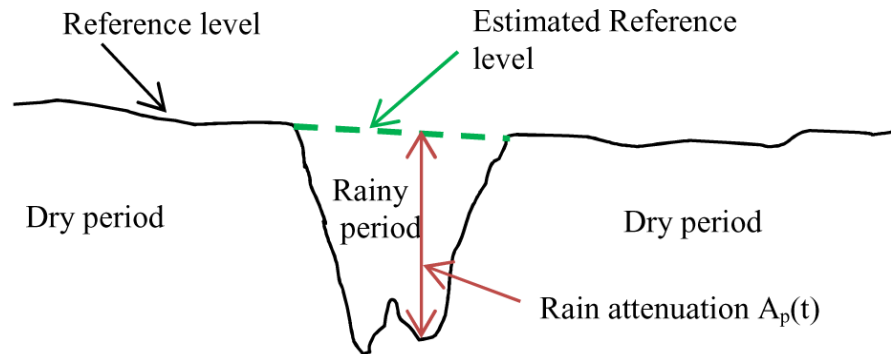


Fig. 5. Example of obtained time series: received signal (blue curve), radar rain rate (red curve), 1-h accumulated rainfall time series (dash green curve).

[Title Page](#)[Abstract](#)[Introduction](#)[Conclusions](#)[References](#)[Tables](#)[Figures](#)[⏪](#)[⏩](#)[⏴](#)[⏵](#)[Back](#)[Close](#)[Full Screen / Esc](#)[Printer-friendly Version](#)[Interactive Discussion](#)

Rainfall measurement from opportunistic use of earth-space link

L. Barthès and C. Mallet

**Fig. 6.** Received signal during a rain event.

Title Page

Abstract

Introduction

Conclusions

References

Tables

Figures

◀

▶

◀

▶

Back

Close

Full Screen / Esc

Printer-friendly Version

Interactive Discussion

Rainfall measurement from opportunistic use of earth-space link

L. Barthès and C. Mallet

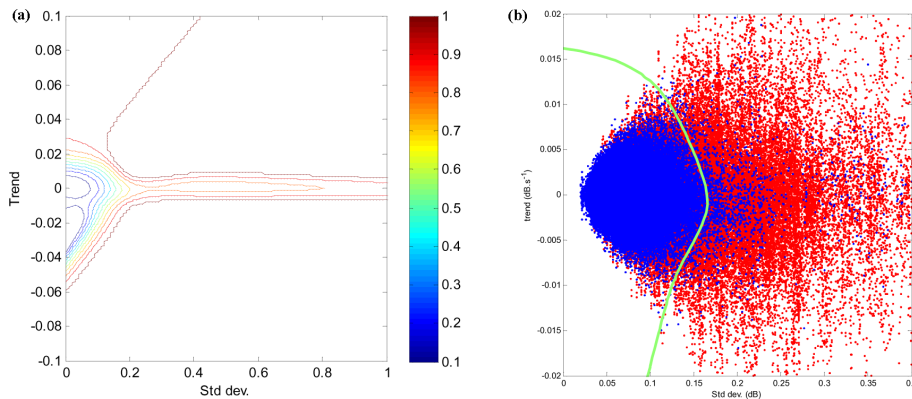


Fig. 7. (a) MLP output: posterior probability of rainy class. (b) Boundary of the classifier (green solid line), samples corresponding to dry class are in blue, samples corresponding to rainy class are in red.

[Title Page](#)[Abstract](#)[Introduction](#)[Conclusions](#)[References](#)[Tables](#)[Figures](#)[◀](#)[▶](#)[◀](#)[▶](#)[Back](#)[Close](#)[Full Screen / Esc](#)[Printer-friendly Version](#)[Interactive Discussion](#)

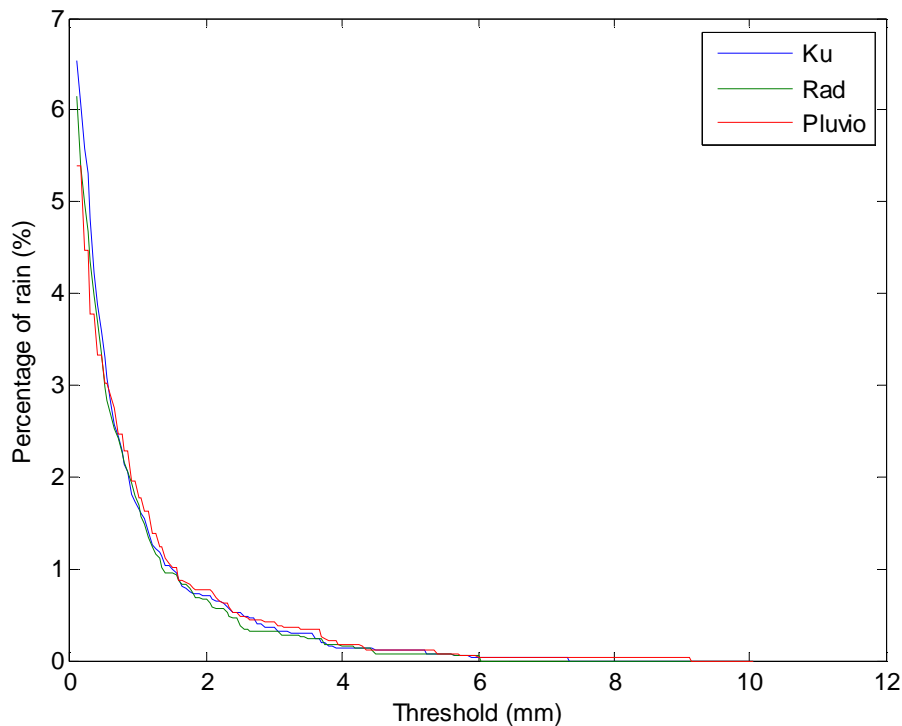


Fig. 8. Percentage of rain vs. 1-h accumulated rain threshold for the radar time series (green), pluviometers (red), Ku device (blue) for a threshold $P_o = 0.55$.

Rainfall measurement from opportunistic use of earth-space link

L. Barthès and C. Mallet

Title Page

Abstract

Introduction

Conclusions

References

Tables

Figures

◀

▶

◀

▶

Back

Close

Full Screen / Esc

Printer-friendly Version

Interactive Discussion



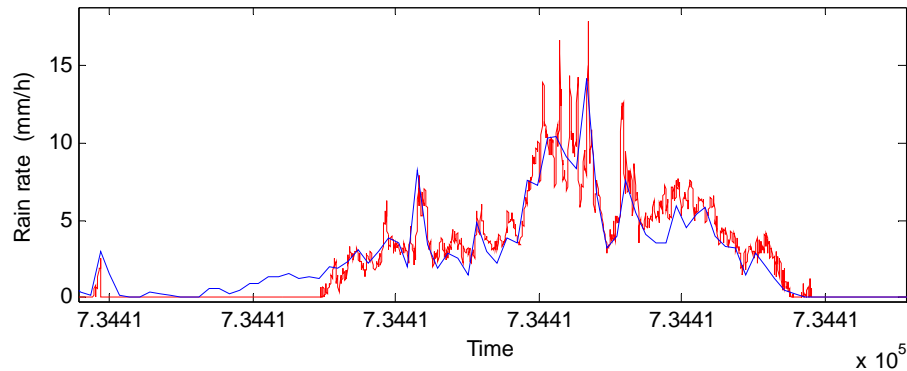


Fig. 9. Example of time series obtained by Ku device (red curve) and Radar (blue curve).

Rainfall measurement from opportunistic use of earth-space link

L. Barthès and C. Mallet

Title Page	
Abstract	Introduction
Conclusions	References
Tables	Figures
⏪	⏩
◀	▶
Back	Close
Full Screen / Esc	
Printer-friendly Version	
Interactive Discussion	

Rainfall measurement from opportunistic use of earth-space link

L. Barthès and C. Mallet

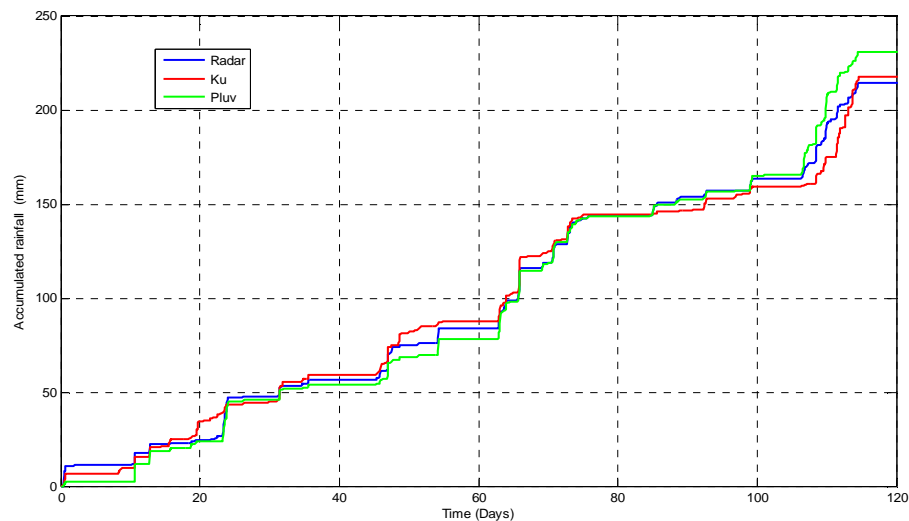


Fig. 10. Accumulated rainfall obtained by radar (blue curve), Pluviometer (green curve), attenuation measurements (red curve) during 4 months.

[Title Page](#)[Abstract](#)[Introduction](#)[Conclusions](#)[References](#)[Tables](#)[Figures](#)[⏪](#)[⏩](#)[◀](#)[▶](#)[Back](#)[Close](#)[Full Screen / Esc](#)[Printer-friendly Version](#)[Interactive Discussion](#)

Rainfall measurement from opportunistic use of earth-space link

L. Barthès and C. Mallet

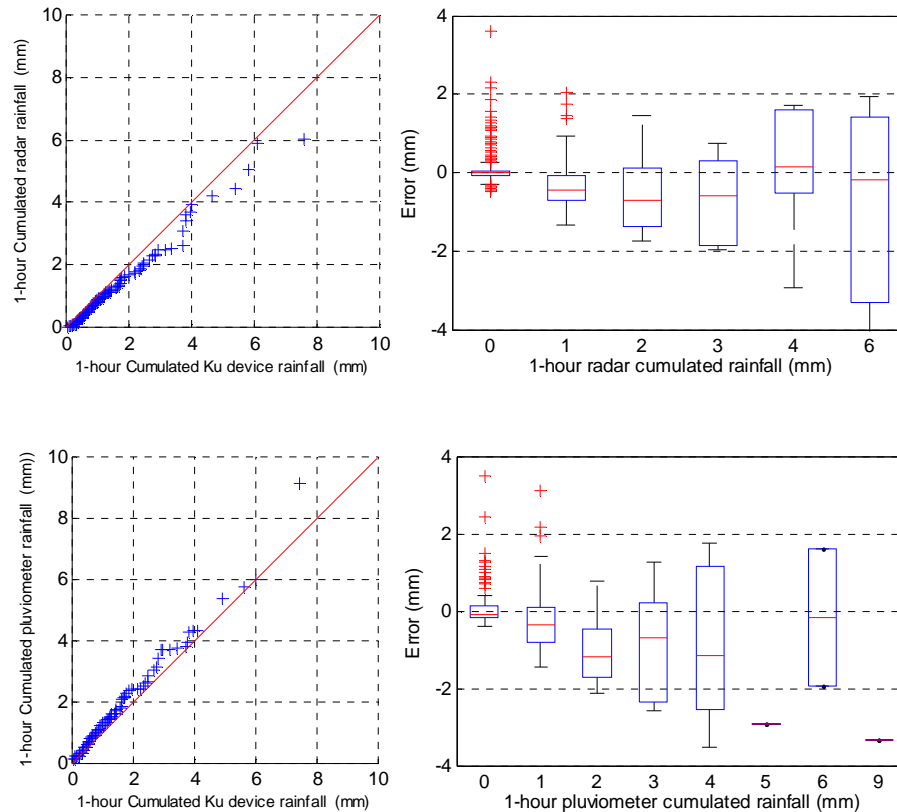


Fig. 11. $Q-Q$ plot between radar and Ku device (top left) and between pluviometers and Ku device (bottom left). Box plot between radar and Ku device (top right) and between pluviometers and Ku device (bottom right).